Seismicity rate and wave-velocity variations as consequences of rainfall; the case of the catastrophic storm of September 2002 in the Nimes Fault region (Gard, France)

A. Rigo, N. Béthoux, F. Masson, J.F. Ritz

Seismicity rate and wave-velocity variations as consequences of rainfall: the case of the catastrophic storm of September 2002 in the Nîmes Fault region (Gard, France)

Alexis Rigo,[1] Nicole Béthoux,[2] Frédéric Masson[3] and Jean-François Ritz[4]

[1] *Laboratoire Dynamique Terrestre et Planétaire,* (UMR 5562), *Observatoire Midi-Pyrénées, Universitéde Toulouse – CNRS,* 14 *Ave. Edouard Belin,* 31400 *Toulouse, France. E-mail: rigo@dtp.obs-mip.fr*

[2] *Géosciences Azur (*UMR 6526*), Université Sophia-Antipolis - CNRS, Nice, France*

[3] *Institut de Physique du Globe de Strasbourg (*UMR 7516*), Université Louis Pasteur – CNRS, Strasbourg, France*

[4] *Laboratoire Géosciences Montpellier (*UMR 5243*), Université Montpellier* II *– CNRS, Montpellier, France*

SUMMARY

The western Provence in southern France is an intraplate low deforming region, cut by large sinistral strike-slip faults as the Nîmes Fault. The deformation rate of this fault was estimated at 0.1 mm yr^{-1} from geological and morphological observations. Nevertheless, some large earthquakes occurred in this area in historical times inducing well-documented partial destructions on the roman monument 'Pont-du-Gard'. In order to investigate if this area is seismically active, we installed a temporary seismological network of 14 stations between the cities of Nîmes and Avignon for a 1-yr period (2002 July–2003 June). We recorded and located a total amount of 80 earthquakes of magnitude Ml smaller than 2.8, and of 153 quarry blasts. The seismic event locations are interpreted in terms of regional tectonics as well as of geometry at depth of the Nîmes Fault and of possible seismic activity of the Roquemaure Fault. At the beginning of 2002 September, a catastrophic storm occurred in the same area with cumulated precipitations at 600 mm in 28 hr, causing casualties and major inundations and damages. We identified a clear and sudden increase of the seismic activity as an immediate consequence of this exceptional meteorological phenomenon. We interpret this rainfall triggering of earthquakes as the response of the crust to an abrupt vertical loading. The geological context of this zone is characterized by the presence of sedimentary basins and of an important karstic network in a calcareous environment allowing the retention of a third of the total rainwater volume during few weeks after the catastrophic storm. Month by month inversion of the seismic wave velocities for only the first 1-km thick layer of the crust allows investigating the influence of the stored water. A clear decrease of both *P*- and *S*-velocities, and an increase of the *Vp/Vs* ratio are evidenced. The variations obtained are at 2, 6 and 4.5 per cent for *P*-, *S*-velocities and *Vp/Vs* ratio, respectively. These variations are discussed in confront of previous studies and can be directly related to the known water volume.

Key words: Time series analysis; Transient deformation; Seismicity and tectonics; Wave propagation.

1 INTRODUCTION

South of France is an intraplate slow deforming region submitted to the far field effect of African–Eurasian collision converging at a rate of around 0.8 cm yr^{-1} (De Mets *et al.* 1990). The deformation is principally located in the Pyrenees and in the Alps mountain ranges where several historical earthquakes of intensities greater than VIII occurred in the last 1000 yr (Lambert & Levret-Albaret 1996). Between these two active mountain belts characterized by thicken crust, sets the Provence region limited to the north by the Massif Central range with a thinned crust and to the south by the Mediterranean Sea with oceanic crust.

Faults and folds affect the Provence region with E–W trending structures corresponding to folds and thrusts, and NE–SW to NNE–SSW trending structures corresponding to active sinistral strike-slip faults. The overall pattern shows a N–S regional compression, which would absorb approximately 1.5 per cent of the African–Eurasian convergence (Schlupp *et al.* 2001). Because of this low deformation rate, the morphology and the activity of these crustal structures are difficult to characterize unambiguously and are still debated (e.g. Sébrier *et al.* 1998; Mattauer 2005).

In the summer 2002, we installed for a 1-yr period a temporary seismological network. Our objective was to observe if seismic activity exists around the Nîmes Fault, and, if it is the case, what is
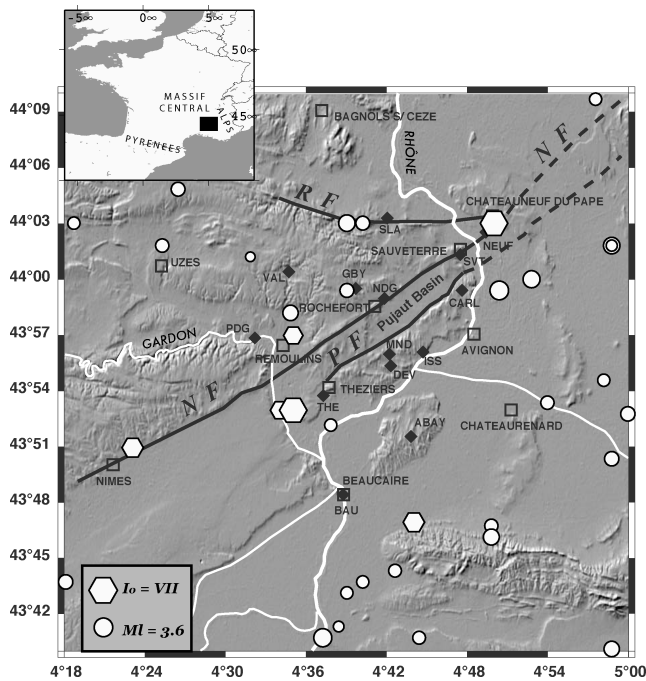
Figure 1. Historical (1397–1980) and instrumental (1980–2000) seismicity map on a Digital Elevation Model from SRTM shuttle mission. Black diamonds: seismological stations of the temporary network (2002 July–2003 June). NF: Nîmes Fault; PF: Pujaut Fault; RF: Roquemaure Fault. Inset: localization of the studied area in France.

its relationship with the faults and the regional tectonics. We then selected the area delimited to the west by the city of Remoulins where the roman monument 'Pont-du-Gard' is located, to the east and to the north by the city of Châteaunauf-du-Pape and to the south by the city of Beaucaire (Fig. 1). This choice was guided by: (i) the occurrence of historical seismic events of intensities greater than VI as in 1769 near Avignon ($I_0 = \mathrm{VII}$) and in 1946 south of Remoulins ($I_0 = \mathrm{VI–VII}$), (ii) the presence of three faults with clear morphology and (iii) to avoid installing seismological stations in the alluvial deposits of the Rhône River, a calcareous area being better conditions to obtain seismological records of good quality.

Two months after installing our temporary network, the 2002 September 8–9, a catastrophic rainfall event affected this area resulting in 24 casualties, the damages being estimated to 1.2 billion euros. As a consequence, the rivers had immediate hydrologic responses with discharges reaching values never seen before (Delrieu *et al.* 2005). According to the rivers, the response was different due to geomorphological factors and to the influence of karst. In fact, the karstic network was saturated and retained a great quantity of water, which was discharged during the following weeks.

The role of fluids in seismological processes is today a subject of great interest. Since a long time, seismicity induced by fluid injection or extraction in reservoirs or by filling up of dams is well known (Grasso & Wittlinger 1990; Grasso *et al.* 1992; Shapiro *et al.* 2006; Utkucu 2006). Fluids and their migration or concentration in the crust are also invoked to explain changes in the stress field around the faults, particularly in the nucleation zone of the earthquakes (Audin *et al.* 2002; Boullier *et al.* 2004; Miller *et al.* 2004). The influence of fluids was also evidenced during post-seismic and interseismic deformation processes (Yamashita 2003; Fialko 2004). Above all, presence of fluids in the crust induces changes of the elastic properties of the crust and, then, of the characteristics of the

seismic wave propagation. Some laboratory experiments were done in order to calibrate *P*- and *S*-wave velocities under different pore pressure (fluid filled materials) and lithostatic pressure conditions (Nur & Simmons 1969; O'Connell & Budiansky 1974). Inversely, the seismic wave velocities are used to characterize crust and fault rheologies affected by fluid pressure (Watanabe 1993; Stern *et al.* 2001).

In this paper, we study the influence of the sudden and intensive rainfall of 2002 September on the upper part of the continental crust. We will show that this meteorological event was so exceptional to clearly modify the rate of seismic activity and the seismic wave velocities in the Nîmes-Avignon area during the three months following the 2-d storm. Especially, the *P*- and *S*-wave velocities were clearly affected in the most superficial part of the crust most probably related to the geological context dominated by a well-developed gallery network in karst. We will then analyse and discuss these results with respect to previous studies focused on fault and on crust mechanical properties in the presence of fluids and pore overpressure.

2 SEISMOTECTONIC SETTING

The Provence region corresponds to a sedimentary cover made of Mesozoic and Cenozoic ages above a Paleozoic crustal basement. The thickness of this sedimentary cover varies from 7 km in the NW Cévennes-Nîmes region to 2 km to the east (Baudrimont & Dubois 1977). During the last 6 Ma, this region was affected by important variations of the sea level inducing the formation of various successive erosion surfaces and canyons (Clauzon 1996), which are used as morphotectonic markers, as the one found at 0.8 km depth near Châteauneuf-du-Pape (Schlupp *et al.* 2001).

At present, the N–S deformation rate is estimated at 0.1 mm yr^{-1} by geological considerations over a period of 20 Ma (Champion *et al.* 2000). Elsewhere, the geodetic estimates of the deformation rate vary from 0.6 to 2 mm yr^{-1} over a wide area including at least the Durance and the Nîmes faults (Ferhat *et al.* 1998; Nocquet & Calais 2003).

The region of our interest is in the centre of the Provence domain, around the city of Avignon, on the western side of the Rhône River (Fig. 1). This zone comprises three major faults: a 65-km-long segment of the Nîmes Fault, the Pujaut Fault and the Roquemaure Fault (respectively NF, PF and RF in Fig. 1). Since Messinian (-5 Ma) age, the Nîmes Fault would have a sinistral strike-slip fault movement at a deformation rate of 0.08 ± 0.01 mm yr^{-1} (Schlupp *et al.* 2001). However, although a paleoseismic evidence was found near Courthézon northeast of Châteauneuf-du-Pape city (Combes *et al.* 1993) showing the occurrence of one, maybe two, seismic ruptures in the past 250 000 yr, no cumulated deformation was observed in the adjacent Miocene deposits suggesting that the deformation rate is extremely low. The Pujaut Fault corresponds to a normal fault with a steep north dipping acting during the Oligo–Miocene time, the northward downthrown footwall being called the Pujaut graben or Pujaut Basin (Fig. 1). Finally, the Roquemaure Fault is a somehow an 'unknown' fault, ignored by much of geologists, being considered either as inexistent or inactive.

In Fig. 1, we also reported historical (1397–1946 period) and instrumental (1980–2000 period) seismicity. The seismicity is diffuse all over the studied area with no immediate relationship between earthquakes and faults. The most relevant historical events are the two 1769 earthquakes ($I_0 = \mathrm{VII}$) so-called 'Avignon earthquakes' but both located at the Châteauneuf-du-Pape city at the tip of the

mapped Nîmes Fault, and the 1946 earthquake ($I_0 =$ VII) southeast of the city of Theziers, in the southward extension of the Pujaut Fault. Archaeological studies of the roman monument 'Pont-du-Gard' evidence successive partial destructions most probably due to seismic events occurred in the centuries I, IV and VI (Combes *et al.* 1997). Over the instrumental period, the seismicity with magnitude Ml ranging between 1.8 and 3.6, is distributed in the entire considered region without clear link with the faults, excepted for two events located on the Roquemaure Fault. Marin *et al.* (2004) estimated that the return time period for a characteristic event of magnitude 5.3 is of 250 yr when for a characteristic event of magnitude 7 is more than 5000 yr on the Nîmes Fault.

3 THE RAINFALL EVENT OF SEPTEMBER 2002

The 2002 September 8–9, this region was affected by a catastrophic storm causing the death of 24 people and economic damages estimated to 1.2 billion euros. The heavy precipitations began the September 8 at 08:00 UT to finish the September 9 at 12:00 UT. This area is part of the hydro-meteorological observatory of the Cévennes-Vivarais region (OHM-CV) managed by LTHE laboratory in Grenoble, which allowed, in collaboration with Météo-France, having numerous collected data and a good knowledge of what happened during this event (Delrieu *et al.* 2005). Particularly, several rain gauges in different parts of the area recorded hourly the precipitation amounts as shown in Fig. 2 for the Remoulins and Châteauneuf-du-Pape stations, two sites corresponding, respectively, to the western and eastern limits of our seismological network (Fig. 1). The cumulated precipitations in the centre of our temporary network (between Nîmes and Pujaut faults) reached the value of 400 mm in 28 hr, when it reached 650–700 mm in the Alès city to the north.

Consequently and with short delays, most important floods affected the major rivers of the region and produced also flash floods of many upstream tributaries. The peak discharges reached values of 5–10 m^3 s^{-1} km^{-2} when the 10-yr return period discharge is typically 2 m^3 s^{-1} km^{-2} for Provence area. According to the measurements done at different parts of the area, these river floods were estimated to correspond to 70–100 per cent of the total amount of rainfall. Especially, it appears that in the karstic area the rainfall water retention capacities should be about 30 per cent. We observed that the karstic network released the stored rainwater and the Pujaut Basin remained inundated over 1–1.5 months after the rainfall event.

4 SEISMOLOGICAL NETWORK

We maintained the seismological network from the beginning of 2002 July to the end of 2003 June. We carried out 14 stations over an area of 34 × 28 km^2 (Fig. 1), but considering various technical problems on the instruments (power supply, inundations, electronic failures), the network had a maximum of 13 and a minimum of 10 simultaneous working stations. In particular, station VAL drown under 2 m of water was stopped during two months (2002 September and October), station MND was definitively stopped in 2002 December consecutively to a complete breakdown and was substituted by station ISS, and station NEUF was stolen in 2003 April (Table A1 in the Appendix).

A station is constituted of a digital recorder with a three component short-period seismometer and a GPS or DCF antenna for
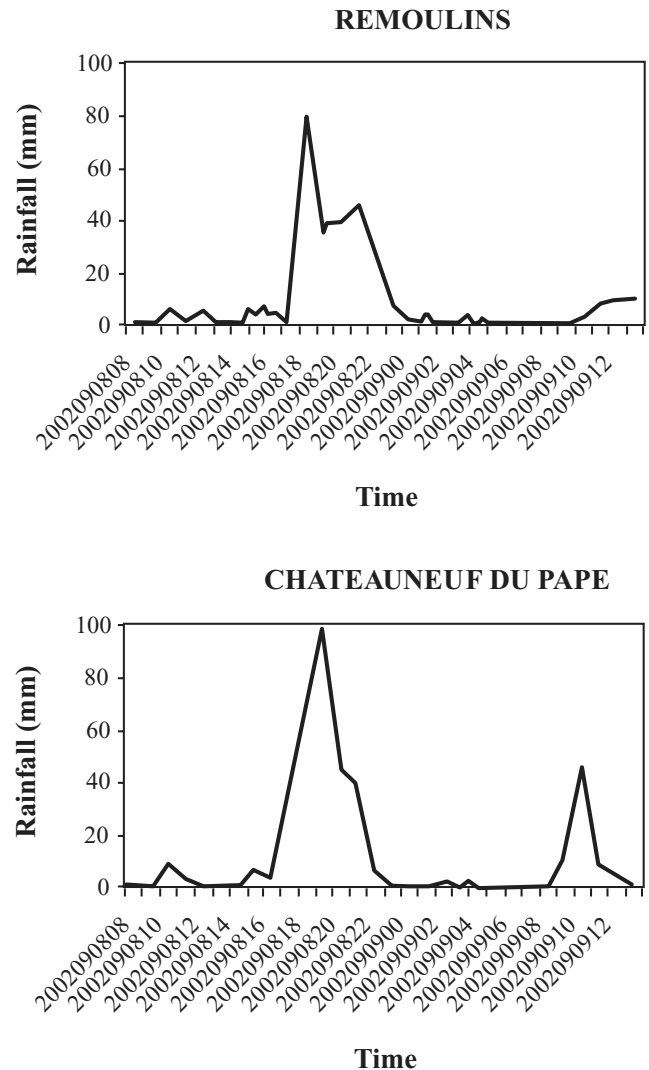

Figure 2. Hourly rainfall measurements in millimetres at two permanent meteorological stations in Remoulins and in Châteauneuf-du-Pape cities (modified from Delrieu *et al.* 2005).

absolute time recorded in parallel with the internal station clock. The stations were in a continuous mode recording with a sampling rate of 125 Hz. Generally the stations were rather noisy, because located in a region of intense economic activities as major railroads, highways, and quarries. Nevertheless, the accuracy of the *P*- and *S*-arrival time readings was estimated to be better than 0.05 s.

5 DATA ANALYSIS

5.1 Preliminary locations

The seismological signals of major amplitude were automatically extracted from the continuous records and the events were separated from noise caused by human activities near the stations. During the period of survey, 15 earthquakes with magnitude Ml ranging from 1.7 to 2.8 were located in the same area by the French permanent networks (Réseau National de Surveillance Sismique—RéNaSS, and Commissariat l'Énergie Atomique/Laboratoire de Détection Géophysique—CEA/LDG, data available on http://www.bcsf.prd.fr/). The magnitude of the

Table 1. 1-D velocity models.

Depth (km)	M1			Vc		
	P-velocity (km s^{-1})	*S*-velocity (km s^{-1})	*Vp/Vs*	*P*-velocity (km s^{-1})	*S*-velocity (km s^{-1})	*Vp/Vs*
0	4.6	2.7	1.73	4.57	2.58	1.77
1	4.9	2.8	1.73	5.16	2.98	1.73
7	5.4	3.1	1.73	5.53	3.10	1.78
12	5.7	3.3	1.73	5.76	3.53	1.63
18	6.0	3.5	1.73	6.26	3.66	1.71
30	8.0	4.7	1.73	7.37	4.37	1.69

Notes: M1: velocity model used with Hypo71 code (Lee & Lahr 1975); *Vc*: final velocity model obtained with the Velest code (Kissling *et al.* 1994) for the 1-yr period of the temporary seismological survey.

other events we detected is fixed to 1 because of the impossibility to determine it precisely.

The first question to solve was to determine a regional 1-D *P*-velocity model unconstrained until now. For that, we used the geological knowledge and the 15 common earthquakes detected by the temporary and the permanent networks. We then fixed a superficial layer of 1 km of thickness corresponding to the sediment filling in the Messinian canyons as those observed near Châteauneuf-du-Pape and Pujaut (Schlupp *et al.* 2001). We also fixed a velocity contrast at 7 km depth corresponding to the maximum thickness of the Mesozoic and Cenozoic cover (Baudrimont & Dubois 1977). Other three velocity contrasts were imposed at 12 km, 18 km and at 30 km depth, this last one being the mean position of the base of the continental crust in France. Our aim was to obtain the minimum residuals for the earthquake locations at both the temporary and permanent seismological stations. Thus, we used Hypo71 code (Lee & Lahr 1975) in a trial-and-error mode, in order to determine a preliminary *P*- (and *S*-) velocity model M1 (Table 1), the *Vp/Vs* ratio being fixed at the common French value of 1.73. To avoid refracted waves, the maximum epicentral distance was imposed at 120 km, the nearest permanent station being approximately at 40 km from the centre of the temporary network.

5.2 Discrimination between seismic events and blasts

The second step was to distinguish the quarry blasts from the seismic events. A first differentiation was done by the specific waveform of blasts recorded at some specific stations. This way allows recognizing 5 per cent of the blasts only. Secondly, we located all the events with the velocity model M1 and we extract from the clusters found, the events occurring approximately at the same hours during the working days and the working hours. This selection of events as quarry blasts was confirmed by a decrease of their location residuals when fixing their depth at 0 km, the locations being at a distance smaller than 5 km from the known quarries. We were then able to locate a final set of 80 earthquakes and 153 quarry blasts with reasonable residuals (smaller than 0.5 s).

5.3 1-D seismic wave velocity model determination

Finally, we inverted simultaneously the *P*- and *S*-velocities and the earthquake locations using the Velest code (Kissling *et al.* 1994). The blast locations were fixed at the quarry positions and at 0 km depth, the thicknesses of the layer of the velocity model were also fixed at the model M1 values. We then obtained the velocity model *Vc* (Table 1). We estimate from several inversion processes varying the number of iterations and modifying the initial velocities that the uncertainties of *P*-, *S*-velocities and of *Vp/Vs* ratio are, respectively,

of 0.05, 0.10 km s^{-1} and 0.06. As the same, the earthquake location uncertainties are estimated at 0.8 km for the epicentral position and at 1 km for the depth location. The determination of a 3-D seismic velocity model was not realistic because of the predominance of quarry blasts respect to the seismic events implying an insufficient sampling of the crust.

6 TEMPORAL VARIATIONS

Among the 80 located earthquakes (Table A2 in the Appendix), only 24 are located in the temporary seismological network, that is, these events have their epicentral position in the surface covered by the temporary network and, thus, are the best located. Figs 3(a) and (b) show the evolution with time over the 1-yr observation period of all the seismicity recorded. These figures reveal a clear increase of the seismic activity just after the rainfall of 2002 September (vertical arrow in Fig. 3), when the mean weekly seismic activity is at around 1–2 earthquakes. Among the 24 in-network earthquakes, 8 events (three of them with magnitudes Ml 1.4, 1.9 and 2.0, Table A2) occurred during the week following the catastrophic rainfall of 2002 September (Fig. 3c). Another aspect of this after-rainfall seismic activity is the predominance of shallower events with depth smaller than 5 km (Fig. 3a), as five of the eight earthquakes occurring the week after the rainfall in the network (Table A2).

Other two specific features can be noticed about this clear rain-triggered seismic activity: (i) the triggering initiates only 15 hr after the end of the storm (event of September, 10 at 3:29 UT, Table A2) at 1.8 km depth and (ii) the events are distributed all over the area of the survey and not concentrated in clusters (Fig. 6). These characteristics are significantly different from the commonly observed seismicity induced by rain and by artificial water reservoirs, specifically named Reservoir-Induced-Seismicity (RIS). First, in both cases, the seismicity is always described as being distributed in clusters with hundreds of events (see Gupta 2002 for a review, Kraft *et al.* 2006a, b), when in our study no swarm is distinguished. Secondly, the time delay between the cause of triggering and the beginning of the induced seismicity is generally days and months and not hours (Gupta 2002). For impoundments of dams, the time delay is 1–3 months (Gupta 2002; do Nascimento *et al.* 2004; Peinke *et al.* 2006), and for rain-triggered seismicity as at Mt. Hochstaufen, SE-Germany is 9–11 d (Kraft *et al.* 2006a).

Although, the triggering mode of this type of seismicity is still in debate, several authors (e.g. Bell & Nur 1978; Gupta 2002) have underlined three main possible mechanisms: (i) the loading effect due to the filling of the reservoirs or of the karstic network inducing an increase of the elastic stress in the crust, (ii) the increase of the pore fluid pressure in response to elastic stress increase and (iii) the pore fluid pressure changes due to fluid migration into the hypocentral
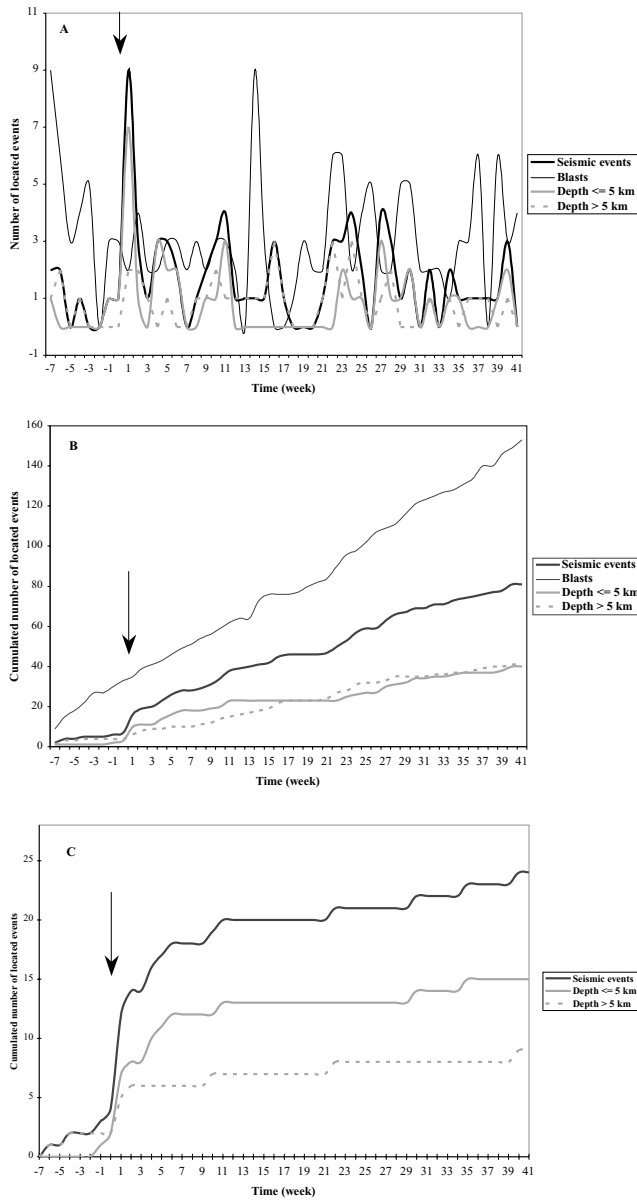
Figure 3. Weekly evolution (the origin of week is the first week of September) of the recorded seismic activity distinguishing seismic events, quarry blasts, earthquakes with depth smaller than 5 km and earthquakes with depth greater than 5 km. (a) Weekly evolution of the seismic activity; (b) The same as (a) in a cumulated diagram; (c) the same as (b) for only the 24 seismic events located in the temporary seismological network. Vertical arrow indicates the occurrence of the catastrophic rainfall of 2002 September 8–9.

Figure 4. Monthly variations of *P*-velocity (top), *S*-velocity (middle) and *Vp*/*Vs* ratio (bottom) for the first 1-km thick layer of the *Vc* velocity model, the yearly values are from *Vc* model (see text for more details). Vertical error bars are standard deviations. Monthly cumulated rainfall is also shown (data from Météo-France).

zone. Most probably the three mechanisms act all together, but with different time delay of response. In fact, it is considered that loading effect generates a rapid response of the seismicity when fluid migration generates the most delayed response. In our study, the seismicity response being very rapid should be considered directly related to a loading effect due to the quantity of rainwater stored in a brief period. Nevertheless, pore fluid pressure diffusion and, maybe, fluid migration, should be responsible for the later seismic events as the $M = 2$ event of October 1 (Table A2).

The inundations and the runoff of the water from the karstic network were observed until the mid of the month of October. The presence of s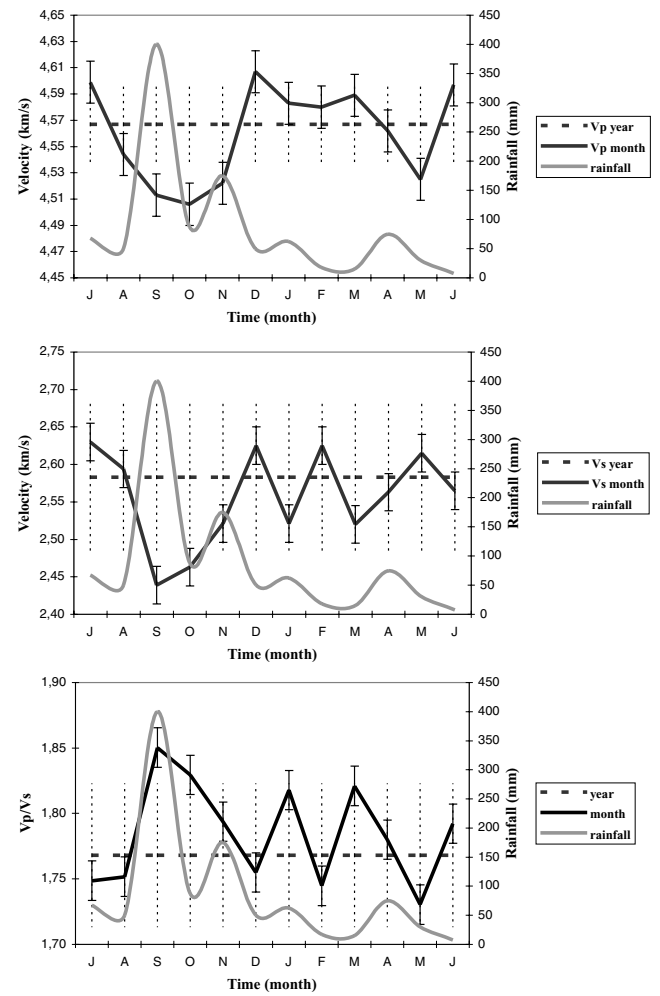uch a quantity of water in the superficial geological layer would have consequences on *P*- and *S*-wave velocities (*Vp* and *Vs*, respectively). We tested this hypothesis inverting month by month the event locations, and *Vp* and *Vs* in only the first layer on the *Vc* model (Table 1) with Velest code. The initial conditions of the inversion are the *Vc* velocity model and the associated event and quarry blast locations. Off the located earthquakes, only three have depths smaller than 1 km, when, obviously, all the quarry blasts are at the surface of the first layer but with fixed locations. The *P*- and *S*-wave velocities for the layers deeper than 1 km are fixed at the *Vc* model values. The changes in the final earthquake locations obtained by this new inversion process are in the uncertainties of those obtained with the *Vc* model and, then, do not modify the pattern of the distribution of the seismicity. The monthly *P*- and *S*-wave velocities, and then the *Vp*/*Vs* ratio obtained for the first 1-km-thick layer vary also in the uncertainties excepted for the months of September, October and November (Fig. 4). The *P*-wave velocity (Fig. 4a) decreases to the value of 4.50 km s^{-1} in September, remains at this level in October and increases to return to its mean value of 4.58 km s^{-1} in November and December. Then, the maximum variation here obtained is 1.5 per cent. The *S*-wave velocity (Fig. 4b) shows the same behaviour with a decrease to a value of 2.45 km s^{-1}
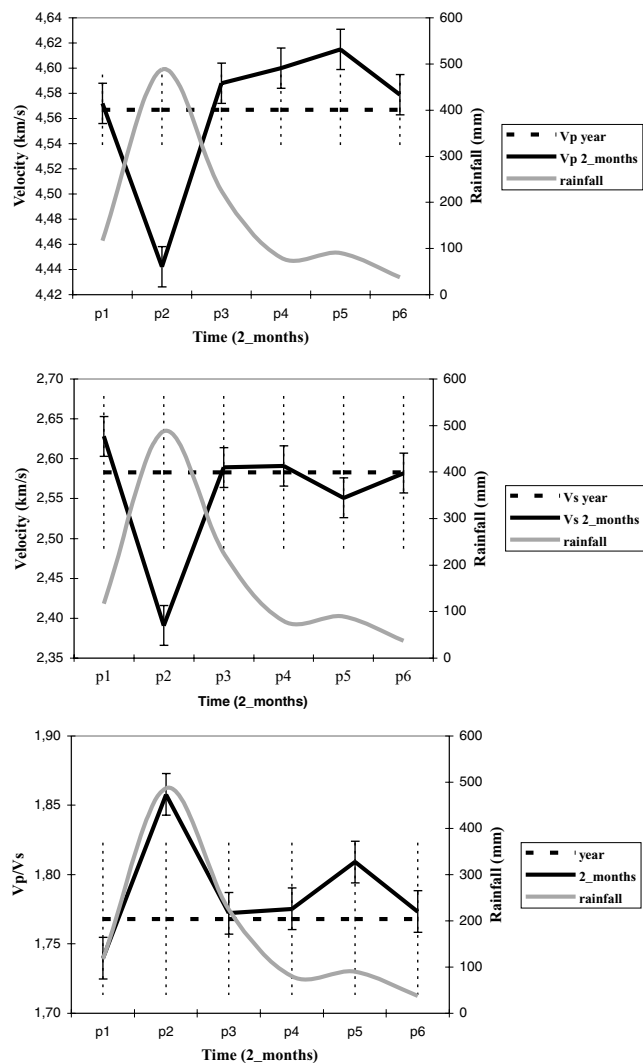
Figure 5. The same as Fig. 4 for the year divided in 6 periods of two months: p1: 2002 July–August; p2: 2002 September–October; p3: 2002 November–December; p4: 2003 January–February; p5: 2003 March–April; p6: 2003 May–June.

when the mean value is 2.58 km s^{-1}, implying a maximum variation of 5.5 per cent. The S-wave velocity returned to its mean value in November more rapidly than the P-wave velocity. Thus, the Vp/Vs ratio (Fig. 4c) shows an abrupt increase in September to the value of 1.85 when the mean value for the year is 1.77, that is, a maximum variation of 4.5 per cent. As it can be noticed, Vs and the Vp/Vs ratio show oscillations after November. These oscillations are due to the small number of events (a mean of 20 events, i.e. earthquakes and blasts) used to invert the velocity model at each month. The Vp/Vs oscillations are principally related to the oscillations of Vs for which the arrival times used are less precise and less numerous than for Vp. In fact, the oscillations disappear when we subdivide the year in six periods of 2 months, increasing the data used for each inversion as shown in Fig. 5. This last figure also confirms the clear decrease of the P- and S-wave velocities and the increase of the Vp/Vs ratio just after the storm of September.

We then suggest that these variations of the wave velocities are clearly related to the rainfall event and, then, to the filling of the local karstic network and the saturation of the ground waters. The return of the wave velocities to their mean values in November

and not in October as it would be expected, is most probably due to new episodes of rainfall in November delaying the flowing of the water stored in September.

7 SEISMIC EVENTS DISTRIBUTION

The final locations of the earthquakes is shown in Fig. 6 and listed in Table A2. It is also shown the P-residuals (NS bars, positive to the north) and S-residuals (EW bars, positive to the east) at each station. The mean values are 0.1 s and 0.3 s for P- and S-residuals, respectively. The most important residues are found at the stations NEUF and ABAY. For the first one, these high values are due to the location of the station in the Rhône River valley on alluvial terraces, and for the second one they are most probably due to a local site effect.

The seismicity distribution appears quite similar to that observed with the historical and instrumental seismicity (Fig. 1) with no immediate evidence of relationship between seismic events and faults. Especially, the seismic activity occurring between the cities of Remoulins and Rochefort, and near the stations of SLA and THE, seems to be a permanent feature through time. The earthquake with largest magnitude (Ml = 2.8; 2003 April 6, Table A2) well felt by inhabitants is located east of station THE where earthquakes occurred in historical and instrumental times. The same observation should be done for the area around SLA station on the Roquemaure Fault. A specific feature concerns the events located north to the city of Châteauneuf-du-Pape. This activity is in an area including three quarries named J, K and L (Fig. 6). These events were analysed with great caution and they are effectively considered as seismic events because (i) some of them are detected by permanent stations, (ii) others occurred in not working hours and days and (iii) for the events out of the two first circumstances, the location residuals are greater than 1–1.5 s when they are fixed on the quarry positions.

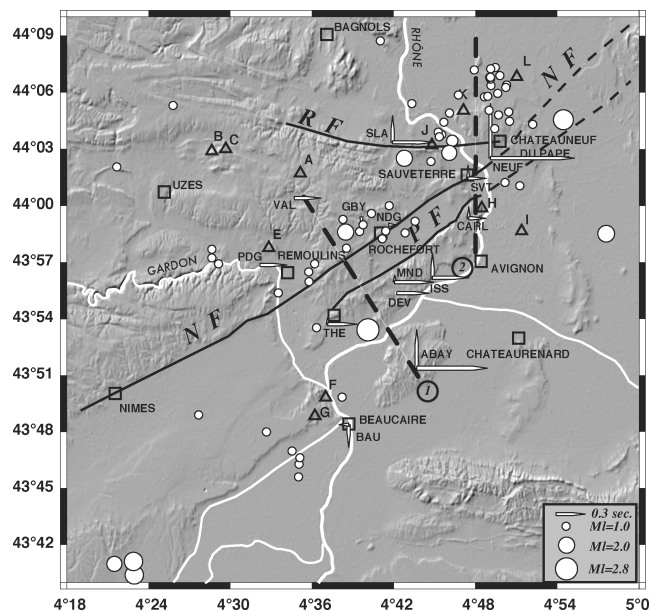**Figure 6.** Map of the final location of the seismic events recorded by the temporary seismological network over the 1-yr period (2002 July–2003 June). The P-residuals (NS bars, positive to the north) and S-residuals (EW bars, positive to the east) are given at each seismological station. Triangles quoted (a) to (g) locate the quarries. Dotted lines named 1 and 2 indicate the position of the two cross-sections shown in Fig. 8.
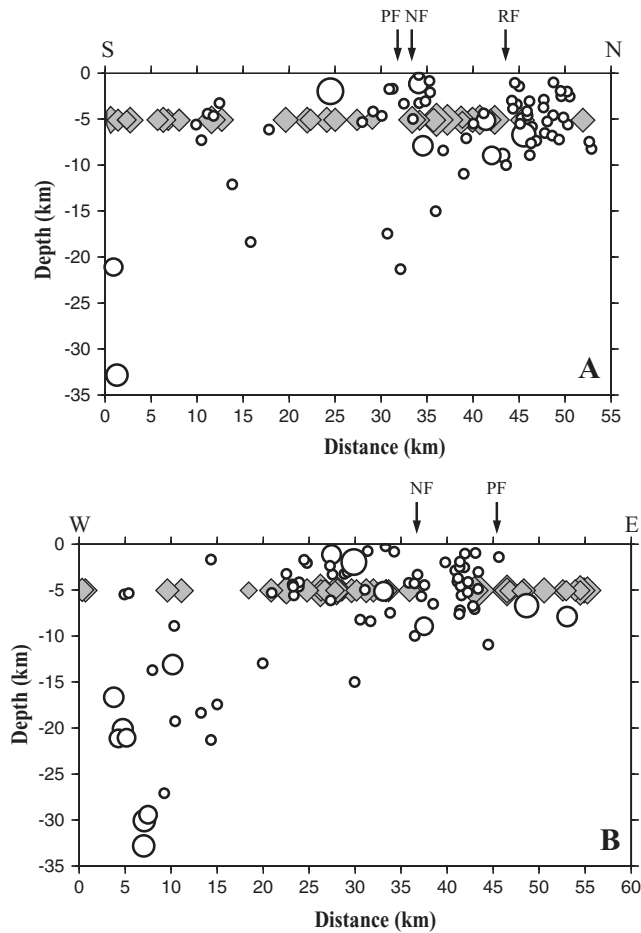
Figure 7. NS (a) and EW (b) cross-sections cutting at the centre of the temporary seismological network with all the seismic events projected. Shaded diamonds are the instrumental earthquakes (data from the French permanent seismological network—Bureau Central Sismologique Français—BCSF). Vertical arrows locate the surface traces of the faults: NF: Nîmes Fault, PF: Pujaut Fault and RF: Roquemaure Fault.

We present in Fig. 7, NS and EW cross-sections with all the events projected, the shaded diamonds being the historical and instrumental seismicity for which depths are unconstrained and fixed to 5 km. If a major part of the 2002–2003 observed events have depths smaller than 10 km, few earthquakes are located at depths between 10 and 20 km, and few at depths greater than 30 km. These last ones located south of the city of Nîmes being out of and far from the temporary network, their depths have greater uncertainties and they are, therefore, difficult to interpret. Then, the major part of the observed seismic activity takes place in the sedimentary cover of Mesozoic and Cenozoic ages.

In order to analyse more precisely the seismicity located in the network and its relationship with the faults, we realize two other cross-sections with a half-band width of projection of 9 km, indicated as 1 and 2 on Fig. 6 and shown in Fig. 8. On both sections, no earthquakes are associated with the Pujaut Fault for which we have poor knowledge on the geometry at depth. Some events can be linked to the Nîmes Fault plane at depth. The geometry at depth of this fault deduced from seismic images is considered as a vertical plane until 5 km at maximum and flattened to the SE (Benedicto *et al.* 1996). Section 1 (Fig. 8a) may confirm that the Nîmes Fault plane is vertical until at least 5 km depth, when section 2 (Fig. 8b)
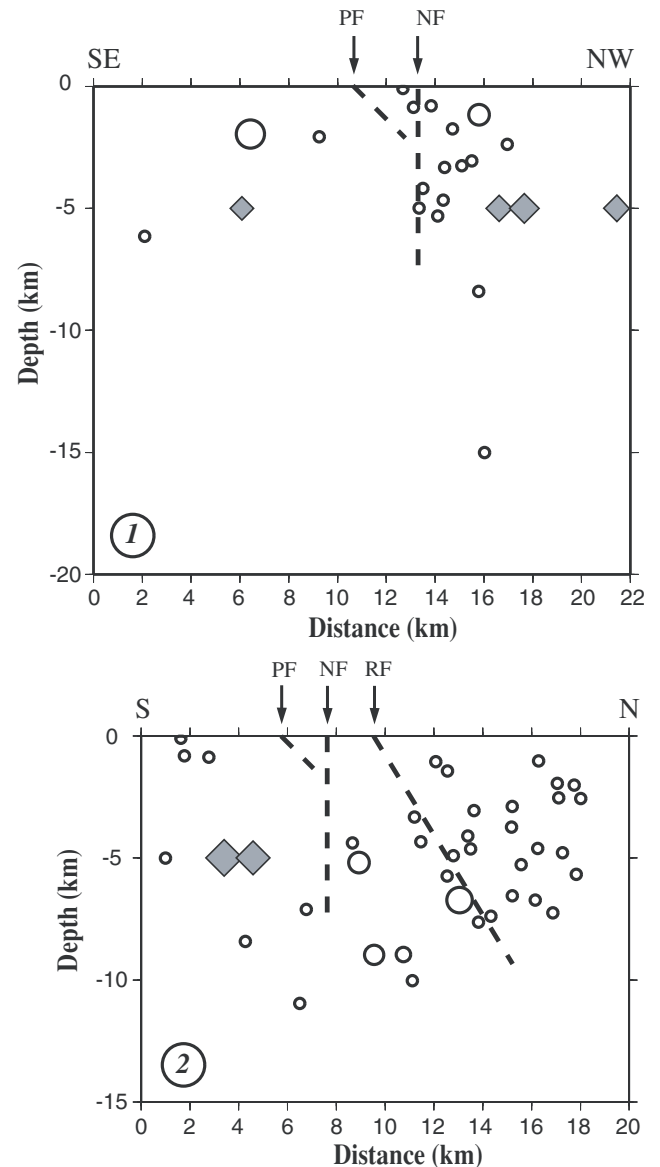
Figure 8. Cross-sections 1 and 2 located in Fig. 6. Symbols and abbreviations are the same as Fig. 7. PF plane is drawn with a dip of 45° and RF plane with a dip of 60°.

shows seismicity sparser and maybe related to the Nîmes Fault until 10 km depth. In any case, it is impossible here to image and to confirm the low-angle geometry at depth of the Nîmes Fault as proposed by Benedicto *et al.* (1996). As concerns the Roquemaure Fault, Section 2 (Fig. 8b) shows seismicity north to the fault with a dip to the north. This suggests that the Roquemaure Fault might have some activity contrarily to what was considered until now. The observed activity is located to its eastward apparent termination. It might be also triggered by the rainfall event of September.

8 DISCUSSION AND CONCLUSIONS

8.1 What about the geometry and activity of faults?

Maintaining a temporary seismological network of 10–13 stations over a 1-yr period (2002 July–2003 June) in the Provence region between the cities of Nîmes and Avignon (southeast of France), we

precisely located 80 earthquakes with magnitude Ml smaller than 2.8 and with depths mainly smaller than 10 km. The distribution of these events seems to follow a SW–NE trend parallel to the Nîmes Fault direction (Fig. 6). As also seen on the cross-sections (Figs 7 and 8), only a part of this seismic activity seems to be linked to the Nîmes Fault and the Roquemaure Fault. Our observations do not allow to confirm if the southwestern part of the Nîmes Fault is really active today despite the suspicion that it was responsible of earthquakes damaging the roman aqueduct 'Pont-du-Gard' in historical times. However, the observed seismicity suggests that its central part is still active, already postulated from the distribution of both historical and instrumental events (Fig. 1). Concerning the geometry of the faults at depth, our data shows that the Nîmes Fault is vertical until 5 km depth and that the Roquemaure Fault may have some activity within its eastern termination when two earthquakes are associated to its central part (1986 June 18 Ml = 2.6; 1997 June 26 Ml = 3.1—Fig. 1). The event distribution at depth shows a possible dip of 50–60° to the north until 10 km depth (Fig. 8).

8.2 A triggering effect of rainfall

Among the 80 located events, 24 are in the network for which 11, that is, 40 per cent, occurred during the two weeks following the catastrophic rainfall of 2002 September 8–9. There is a clear link between this meteorological event and the triggering of the earthquakes (Fig. 3). As mentioned before, three mechanisms are invoked to explain the triggering of earthquakes by artificial water reservoir filling or by rainfalls. The time delay separating the formal cause of the triggering and the occurrence of the first earthquake allows distinguishing in between these three processes. In commonly studied cases (Gupta 2002), the mechanism admitted is the pore fluid pressure change at hypocentral depths due to fluid migration. This mechanism is timely controlled by the pore pressure diffusion, the increase of the seismicity having commonly a delay of 1–3 months after a specific event concerning water reservoir level (filling or discharge), the known shorter delay being at 10 d in the case of the rainfall-triggered earthquakes in the SE Germany (Hainzl et al. 2006; Kraft et al. 2006a). In our study, the triggering of earthquakes initiates 15 hr after the end of the storm excluding a pore fluid diffusion. The most important consequence of the great quantity of fallen water is an abrupt vertical loading on the ground surface. If we consider a high porosity for the 0.8-km-thick sediment filling up of the Messinian canyons (Schlupp et al. 2001) associated with a well-developed karstic network, that might correspond to a 800 m water column at maximum, and then to a maximum overpressure of 80 bars (or 8 MPa). This is largely sufficient to trigger seismic activity in the first kilometres of the crust. In fact, stress variations deduced from static Coulomb Failure Function have generally triggering earthquake thresholds of about 0.1 bar (e.g. Reasenberg and Simpson 1992). An example of triggering earthquakes due to vertical loading on the ground was observed after the construction of the Taipei 101 tower (Taiwan). In this case, the vertical loading was estimated to be 'only' 5 bars (0.5 MPa), clearly sufficient to trigger seismicity until 10 km depth (Lin 2005). If we consider this value of 5 bars for the vertical loading in our case study in the French Provence as reasonable and sufficient to trigger the observed seismicity until 8 km depth, that corresponds to a 50 m water column, which seems to be also reasonable and perhaps more consistent with the geological and the meteorological contexts. Moreover, in our study, we can consider two categories of earthquakes following Simpson et al. (1988). (i) The 'rapid response' category including

the earthquakes occurring the two weeks after the storm, and for which the triggering is linked to the vertical loading of the rainwater on the ground. The stress increase might be transferred into the upper crust (2–5 km depth) due to soft sediments and, maybe, to fluid saturated rocks, vertical stress diffusing more rapidly than pore fluid. (ii) The 'delayed response' category for the events occurring in the weeks following, where stress variations due to the previous earthquakes, pore fluid diffusion and fluid migration act. In any considered case, it seems clear that the triggered seismicity is facilitated by the pre-existing faults and associated fractures in the upper crust.

8.3 A wave-velocity variation effect

At least a third of the total volume of rainfall water of the September storm was stored saturating the ground water reservoirs and the galleries of the karst (Delrieu et al. 2005). We observed that this stored water was released during 1.5 months after the storm. Such saturation of the superficial part of the crust should have consequences on the seismic wave velocities (Nur & Simmons 1969; O'Connell & Budiansky 1974; Husen & Kissling 2001; Stern et al. 2001). We tested this hypothesis and we found a significant decrease of wave velocities in the first 1-km-thick layer of our Vc velocity model determined for the 1-yr observation period (Fig. 4). Both P- and S-wave velocities are affected during the months of September, October and with less evidences of November. As observed by Husen & Kissling (2001) in Chile for the 1995, $M_W = 6.6$ Antofagasta earthquake, the decrease of S-velocity is more important than of P-wave velocity decrease implying an increase of the Vp/Vs ratio.

Husen & Kissling (2001) and Stern et al. (2001) showed variations of Vp/Vs ratio and P-wave velocity at around 6–10 per cent. In our study, the variations for P-, S-wave velocities and Vp/Vs ratio are 1.5–2, 5–6 and 4–5 per cent, respectively, that is, twice smaller than the previous mentioned studies. Considering a mean cumulated rainfall height of 600 mm over an area of 1500 km^2 (Delrieu et al. 2005), we obtain a water volume of 825×10^6 m^3, a third of this being at least of $250–300 \times 10^6$ m^3 corresponding to the volume of stored water during the first weeks following the catastrophic rainfall. The variations of wave velocities and Vp/Vs ratio detected in the crust are commonly interpreted as variations of pore and fluid pressures without any quantification, except in terms of in or out lithostatic/hydrostatic pressure conditions. This quantification is not possible without its direct measurement, because of the lack of direct correlation between wave velocities and associated fluid volumes. According to our results, we then suggest here that a variation of 5 per cent of S-wave velocity and Vp/Vs ratio and a variation of 2 per cent of P-wave velocity might be due to, at least, a volume of $10^8–10^9$ m^3 of water.

REFERENCES

Audin, L., Avouac, J.-P., Flouzat, M. & Plantet, J.-L., 2002. Fluid-driven seismicity in a stable tectonic context: the Remiremont fault zone, Vosges, France, *Geophys. Res. Lett.,* **29,** 1091.

Baudrimont, A.-F. & Dubois, F., 1977. Un bassin mésogéen du domaine péri-alpin: le Sud-Est de la France, *Bull. Centres Rech. Explor.-Prod. Elf Aquitaine,* **1,** 261–308.

Bell, M.L. & Nur, A., 1978. Strength changes due to reservoir-induced pore pressure and stresses and application to Lake Oroville, *J. geophys. Res.,* **83,** 4469–4483.

Benedicto, A., Labaume, P., Séguret, M. & Séranne, M., 1996. Low-angle crustal ramp and basin geometry in the Gulf of Lion passive margin: Oligocene-Aquitanian Vistrenque graben, SE France, *Tectonics,* **15,** 1192–1212.

Boullier, A.-M., Fujimoto, K., Ohtani, T., Roman-Ross, G., Lewin, E., Ito, H., Pezard, P. & Ildefonse, B., 2004. Textural evidence for recent co-seismic circulation of fluids in the Nojima fault zone, Awaji island, Japan, *Tectonophysics,* **378,** 165–181.

Champion, C., Choukroune, P. & Clauzon, G., 2000. Déformation post-miocène en Provence occidentale, *Geodin Acta,* **13,** 67–85.

Clauzon, G., 1996. Limites de séquences et évolution géodynamique, *Géomorphologie,* **1,** 3–22.

Combes, P., Carbon, D., Cushing, M., Granier, T. & Vaskou, P., 1993. Mise en évidence d'un paléoséisme pléistocène supérieur dans la vallée du Rhône: implications sur la connaissance de la sismicit en France, *C.R. Acad. Sci. Paris,* **317,** 689–696.

Combes, P., Fabre, G., Fiches, J.-L., Gazenbeek, M. & Paillet, J.-L., 1997. L'aqueduc romain de Nîmes et l'enregistrement d'événements sismiques, in *Archéologie et sismicit – Autour d'un grand monument le Pont du Gard,* eds Fiches, J.-L., Helly, B. and Levret, A., APDCA, Sophia-Antipolis, 171 pp.

Delrieu, G. *et al.*, 2005. The catastrophic flash-flood event of 8–9 September 2002 in the Gard region, France: a first case study for the cévennes-vivarais mediterranean hydro-meteorological observatory, *J. Hydrometeor.,* **6,** 34–52.

De Mets, C., Gordon, R.G., Argus, D.F. & Stein, S., 1990. Current plate motions, *Geophys. J. Int.,* **101,** 425–478.

Do Nascimento, A.F., Cowie, P.A., Lunn, R.J. & Pearce, R.G., 2004. Spatio-temporal evolution of induced seismicity at Açu reservoir, NE Bazil, *Geophys. J. Int.,* **158,** 1041–1052.

Ferhat, G., Feigl, K., Ritz, J.-F. & Souriau, A., 1998. Geodetic measurement of tectonic deformation in the southern Alps and Provence, France, *Earth planet. Sci. Lett.,* **159,** 35–46.

Fialko, Y., 2004. Evidence of fluid-filled upper crust from observations of postseismic deformation due to the 1992 Mw7.3 Landers earthquake, *J. geophys. Res.,* **109,** B08401.

Grasso, J.-R. & Wittlinger, G., 1990. 10 years of seismic monitoring over a gas field area, *Bull. seism. Soc. Am.,* **80,** 450–473.

Grasso, J.-R., Guyoton, F., Fréchet, J. & Gamond, J.-F., 1992. Triggered earthquakes as stress jauge: implication for the uppercrust behavior in the Grenoble area, France, *Pageoph,* **139,** 579–605.

Gupta, H.K., 2002. A review of recent studies of triggered earthquakes by artificial water reservoirs with special emphasis on earthquakes in Koyna, India, *Earth-Sci. Rev.,* **58,** 279–310.

Hainzl, S., Kraft, T., Wassermann, J., Igel, H. & Schmedes, E., 2006. Evidence for rainfall-triggered earthquake activity, *Geophys. Res. Lett.,* **33,** L19303, doi:10.1029/2006GL027642.

Husen, S. & Kissling, E., 2001. Postseismic fluid flow after the large subduction earthquake of Antofagasta, Chile, *Geology,* **29,** 847–850.

Kissling, E., Ellsworth, W.L., Eberhart-Phillips, D. & Kradolfer, U., 1994. Initial reference models in local earhquake tomography, *J. geophys. Res.,* **99,** 19 635–19 646.

Kraft, T., Wassermann, J., Schmedes, E. & Igel, H., 2006a. Meteorological triggering of earthquake swarms at Mt Hochstaufen, SE-Germany, *Tectonophysics,* **424,** 245–258.

Kraft, T., Wassermann, J. & Igel, H., 2006b. High-precision relocation and focal mechanism of the 2002 rain-triggered earthquake swarms at Mt Hochstaufen, SE Germany, *Geophys. J. Int.,* **167,** 1513–1528.

Lambert, J. & Levret-Albaret, A., 1996. *Mille ans de séismes en France.* BRGM, Nantes, 78 pp.

Lee, W.H.K. & Lahr, J.C., 1975. HYPO71 (revised): a computer program for determining hypocenter, magnitude and first motion pattern of local earthquakes, *U.S. Geol. Survey Open-File report*, 75–311.

Lin, C.-H., 2005. Seismicity increase after the construction of the world's tallest building: an active blind fault beneath the Taipei 101, *Geophys. Res. Lett.,* **32,** L22313, doi:10.1029/2005GL024223.

Marin, S., Avouac, J.-P., Nicolas, M. & Schlupp, A., 2004. A probabilistic approach to seismic hazard in metropolitan France, *Bull. seism. Soc. Am.,* **94,** 2137–2163.

Mattauer, M., 2005. Commentaires à la note de D.Chardon et O.Bellier, *Bull. Soc. Géol. France,* **176**(1), 121–123.

Miller, S.A., Collettini, C., Chiaraluce, L., Cocco, M., Barchi, M. & Kaus, B.J.P., 2004. Aftershocks driven by a high-pressure CO_2 source at depth, *Nature,* **427.** 724–727.

Nocquet, J.-M. & Calais, E., 2003. Crustal velocity field of western Europe from permanent GPS array solutions, 1996–2001, *Geophys. J. Int.,* **154,** 72–88.

Nur, A. & Simmons, G., 1969. The effect of saturation on velocity in low porosity rocks, *Earth planet. Sci. Lett.,* **7,** 183–193.

O'Connell, R.J. & Budiansky, B., 1974. Seismic velocities in dry and saturated cracked solids, *J. geophys. Res.,* **79,** 5412–5426.

Peinke, J., Matcharashvili, T., Chelidze, T., Gogiashvili, J., Nawroth, A., Lursmanashvili, O. & Javakhishvili, Z., 2006. Influence of periodic variations in water level on regional seismic activity around large reservoir: field data and laboratory model, *Phys. Earth planet. Int.,* **156,** 130–142.

Reasenberg, P.A. & Simpson, R.W., 1992. Response of regional seismicity to the static stress change produced by the Loma Prieta earthquake, *Science,* **407,** 69–72.

Schlupp, A., Clauzon, G. & Avouac, J.-P., 2001. Mouvement post-messinien sur la faille de Nîmes: implications pour la sismotectonique de la Provence, *Bull. Soc. Géol. France,* **172,** 697–711.

Sébrier, M., Bellier, O., Peulvast, J.-P. & Vergély, P., 1998. Commentaire la note de Robin Lacassin, Bertrand Meyer, Lucilla Benedetti, Rolando Armijo et Paul Tapponnier «Signature morphologique de l'activit de la Faille des Cévennes (Languedoc, France)», *C. R. Acad. Sci. Paris,* **327,** 855–856.

Shapiro, S.A., Kummerow, J., Dinske, C., Asch, G., Rothert, E., Erzinger, J., Kümpel, H.-J. & Kind, R., 2006. Fluid induced seismicity guided by a continental fault: injection experiment of 2004/2005 at the German Deep Drilling Site (KTB), *Geophys. Res. Lett.,* **33,** L01309, doi:10.1029/2005GL024659.

Simpson, D.W., Leith, W.S. & Scholz, C.H., 1988. Two types of reservoir induced seismicity, *Bull. seism. Soc. Am.,* **78,** 2025–2040.

Stern, T., Kleffmann, S., Okaya, D., Scherwath, M. & Bannister, S., 2001. Low seismic-wave speeds and enhanced fluid pressure beneath the Southern Alps of New Zealand, *Geology,* **29,** 679–682.

Utkucu, M., 2006. Implications for the water level change triggered moderate (M $\geq$ 4.0) earthquakes in Lake Van basin, Eastern Turkey, *J. Seismol.,* **10,** 105–117.

Watanabe, T., 1993. Effects of water and melt on seismic velocities and their application to characterization of seismic reflectors, *Geophys. Res. Lett.*, **20,** 2933–2936.

Yamashita, T., 2003. Regularity and complexity of aftershock occurrence due to mechanical interactions between fault slip and fluid flow, *Geophys. J. Int.,* **152,** 20–33.

APPENDIX A: TABLES

Seismological stations (Table A1) and seismic events (Table A2).

Table A1. Name, location and operational comments of the temporary seismological stations.

Code station	Latitude (°N)	Longitude (°E)	Altitude (m)	Comments
ABAY	43.8590	4.7290	151	Frequent night interruptions for power deficiencies
BAU	43.8070	4.6448	80	
CARL	43.9902	4.7922	132	
DEV	43.9225	4.7040	110	
GBY	43.9917	4.6605	241	Power problems in October and November
ISS	43.9350	4.7438	133	Installed in December following interruption of MND
MND	43.9311	4.7028	109	Damaged by September rainfall – Interrupted in December for power deficiencies
NDG	43.9833	4.6967	156	GPS time cable damaged in January and April
NEUF	44.0422	4.8218	80	Stolen in April
PDG	43.9478	4.5347	85	
SLA	44.0547	4.6998	92	
SVT	44.0222	4.7900	65	Interrupted at the end of April
THE	43.8986	4.6217	85	
VAL	44.0068	4.5791	137	Drown during September rainfall – Interrupted between September and December

Table A2. List of the seismic events located with the monthly velocity models – the 24 highlighted events are located in the network. The events with magnitude greater than 1.0 are those detected and located by the ReNaSS/LDG permanent network.

Date	Hour	Longitude (°N)	Latitude (°E)	Depth (km)	Magnitude Ml	Location rms
02/07/16	10 1	43.9538	4.4773	1.71	1.0	.13
02/07/17	7 35	43.9614	4.4774	21.31	1.0	.11
02/07/22	10 51	43.7690	4.2759	7.31	1.0	.05
02/07/23	**9 20**	**43.7999**	**4.5444**	**12.99**	**1.0**	**.11**
02/08/07	**15 2**	**43.9931**	**4.6729**	**15.02**	**1.0**	**.03**
02/09/01	**5 29**	**43.8922**	**4.6058**	**2.08**	**1.0**	**.08**
02/09/08	**9 29**	**43.9415**	**4.5961**	**4.67**	**1.0**	**.08**
02/09/10	**3 29**	**43.9487**	**4.6032**	**1.75**	**1.0**	**.11**
02/09/10	**7 23**	**43.9625**	**4.6423**	**3.33**	**1.0**	**.03**
02/09/12	10 33	44.0418	4.7131	5.18	2.0	.11
02/09/12	21 1	44.0573	4.7717	8.95	1.4	.25
02/09/12	22 33	44.0465	4.7682	8.96	1.9	.11
02/09/13	**1 3**	**43.9771**	**4.6585**	**3.26**	**1.0**	**.04**
02/09/14	0 4	44.0343	4.3613	5.51	1.0	.09
02/09/14	**5 34**	**43.9329**	**4.5965**	**4.19**	**1.0**	**.01**
02/09/15	**8 25**	**43.9832**	**4.6628**	**3.06**	**1.0**	**.04**
02/09/16	**10 51**	**43.9777**	**4.6902**	**0.81**	**1.0**	**.09**
02/09/17	9 56	44.0204	4.8362	7.10	1.0	.09
02/09/20	**9 52**	**44.0001**	**4.6945**	**8.41**	**1.0**	**.18**
02/09/27	9 54	43.9486	4.4857	17.46	1.0	.02
02/09/30	**0 45**	**43.9862**	**4.7264**	**0.86**	**1.0**	**.05**
02/10/01	15 8	44.1218	4.8245	2.56	1.0	.17
02/10/01	**22 13**	**43.9768**	**4.6411**	**1.18**	**2.0**	**.24**
02/10/07	8 41	44.0745	4.8420	4.89	1.0	.08
02/10/10	21 4	44.0758	4.9079	6.71	2.5	.19
02/10/13	**17 45**	**43.9760**	**4.7141**	**0.09**	**1.0**	**.02**
02/10/15	5 53	44.0719	4.8701	1.43	1.0	.06
02/10/18	**14 30**	**44.0389**	**4.7456**	**4.38**	**1.0**	**.11**
02/10/31	12 23	44.0885	4.4299	8.93	1.0	.09
02/11/06	14 7	44.1064	4.8383	1.08	1.0	.09
02/11/08	10 55	44.0977	4.7792	6.55	1.0	.07
02/11/13	**10 45**	**43.7601**	**4.5835**	**5.55**	**1.0**	**.04**
02/11/13	16 29	44.1147	4.8300	4.82	1.0	.06
02/11/14	16 7	44.1043	4.8372	6.74	1.0	.04
02/11/19	18 1	44.1207	4.8189	5.69	1.0	.07
02/11/20	16 15	44.0827	4.8409	3.18	1.0	.06
02/11/21	8 23	44.0817	4.7685	4.62	1.0	.02
02/11/22	**1 21**	**43.9878**	**4.6379**	**2.12**	**1.0**	**.03**

Table A2 *(Continued.)*

Date	Hour	Longitude (°N)	Latitude (°E)	Depth (km)	Magnitude Ml	Location rms
02/11/25	9 39	44.0900	4.7223	7.39	1.0	.05
02/12/02	7 0	43.5825	4.4202	13.18	2.1	.22
02/12/14	20 7	44.3890	4.7981	13.79	1.0	.09
02/12/21	7 8	43.6315	4.3389	16.63	2.1	.13
02/12/28	10 23	43.6469	4.3561	19.69	2.2	.22
02/12/28	10 32	43.6730	4.3827	30.25	2.3	.06
02/12/28	10 34	43.6651	4.3475	21.28	1.9	.10
02/12/30	13 56	43.6422	4.3923	13.82	1.0	.15
03/01/31	6 45	43.6850	4.3815	32.84	2.3	.12
03/02/06	17 27	44.1454	4.6838	8.25	1.0	.13
03/02/09	**0 58**	**43.9228**	**4.5589**	**5.33**	**1.0**	**.10**
03/02/09	2 25	43.6387	4.3868	29.43	1.9	.15
03/02/11	9 23	43.7712	4.5843	4.43	1.0	.13
03/02/13	10 32	43.7769	4.5851	4.67	1.0	.09
03/02/15	7 37	43.6479	4.4088	27.10	1.0	.10
03/02/17	4 18	44.0626	5.0554	3.86	1.0	.24
03/02/17	11 14	44.1963	4.3699	5.36	1.0	.03
03/02/20	3 56	43.6827	4.3583	21.08	1.9	.16
03/02/20	11 52	43.6013	4.4224	19.29	1.0	.16
03/02/25	12 0	44.1060	4.8191	4.60	1.0	.06
03/02/27	13 51	44.1116	4.8186	7.24	1.0	.06
03/03/10	17 44	44.0960	4.8111	2.96	1.0	.06
03/03/11	11 2	44.0681	4.8237	1.08	1.0	.15
03/03/12	20 47	44.1132	4.8175	2.60	1.0	.11
03/03/16	9 6	43.9752	4.9601	7.96	2.1	.19
03/03/17	16 55	44.0990	4.8275	5.33	1.0	.12
03/03/18	11 5	44.0627	4.7587	3.47	1.0	.19
03/03/20	11 9	44.0737	4.7616	5.70	1.0	.08
03/03/26	10 19	44.0649	4.7547	4.43	1.0	.14
03/04/06	**1 28**	**43.8902**	**4.6687**	**1.97**	**2.8**	**.19**
03/04/14	22 59	44.0842	4.8168	7.62	1.0	.12
03/04/15	10 44	44.1198	4.7988	2.01	1.0	.16
03/04/29	7 30	44.1486	4.2873	7.46	1.0	.05
03/04/30	9 35	43.7830	4.5758	3.28	1.0	.11
03/05/05	**0 36**	**43.9708**	**4.6862**	**5.00**	**1.0**	**.03**
03/05/14	8 53	44.0608	4.7560	10.02	1.0	.07
03/05/22	9 42	43.8150	4.4613	18.38	1.0	.26
03/05/28	14 25	44.0177	4.8545	10.95	1.0	.04
03/06/06	8 38	44.0965	4.8153	3.73	1.0	.02
03/06/10	10 59	44.0801	4.8285	4.15	1.0	.20
03/06/11	**20 12**	**43.8306**	**4.6368**	**6.16**	**1.0**	**.15**
03/06/13	7 23	44.1133	4.8186	1.94	1.0	.11